DATA REPOSITORY ITEM DR2009101

Supplemental Online Material

Reconstructing Earth's surface oxidation across the Archean-Proterozoic transition

Stratigraphy

The ~2,650 to ~2,100 Myr Transvaal Supergroup rests unconformably on the volcano-sedimentary Ventersdorp Supergroup (Fig. DR1 and DR2). It formed during slow regional cooling and subsidence of the Kaapvaal Craton (Sumner and Beukes, 2006). Two structural sub basins can be recognized: the Griqualand-West basin, and the Transvaal basin (Fig. 1).

During the first depositional interval, trough-like basins in the Transvaal basin were filled with alluvial and fluvial siliciclastic rocks (Button, 1973a; Eriksson et al., 2005; Sumner and Beukes, 2006). These continental deposits are equivalent to a marine carbonate-siliciclastic ramp in the Griqualand-West basin (Beukes, 1979, 1987; Sumner and Beukes, 2006). A major disconformity at the top of the interval represents short, but craton-wide exposure of the Ventersdorp basement and lowstand clastic deposition (Fig. DR1; Beukes, 1987; Sumner and Beukes, 2006). Ages of the first depositional interval are relatively well constrained between ~2,650 and ~2,590 Myr. Lavas in the basal Schmitsdrif Subgroup were dated at 2,642±3Myr (Walraven and Martini, 1995); carbonates in the overlying Oaktree Formation gave an age of 2,583±5Myr (Martin et al., 1998) and provide a minimum age for the upper disconformity (Fig. DR1).

As the craton was flooded again, the extensive Malmani-Campbellrand rimmed carbonate platform was established (Fig. DR1; Beukes, 1987; Sumner and Beukes, 2006). Subsidence was higher than in interval 1, but carbonates were able to fill the accommodation space, and thicknesses are uniform over the platform (Sumner and

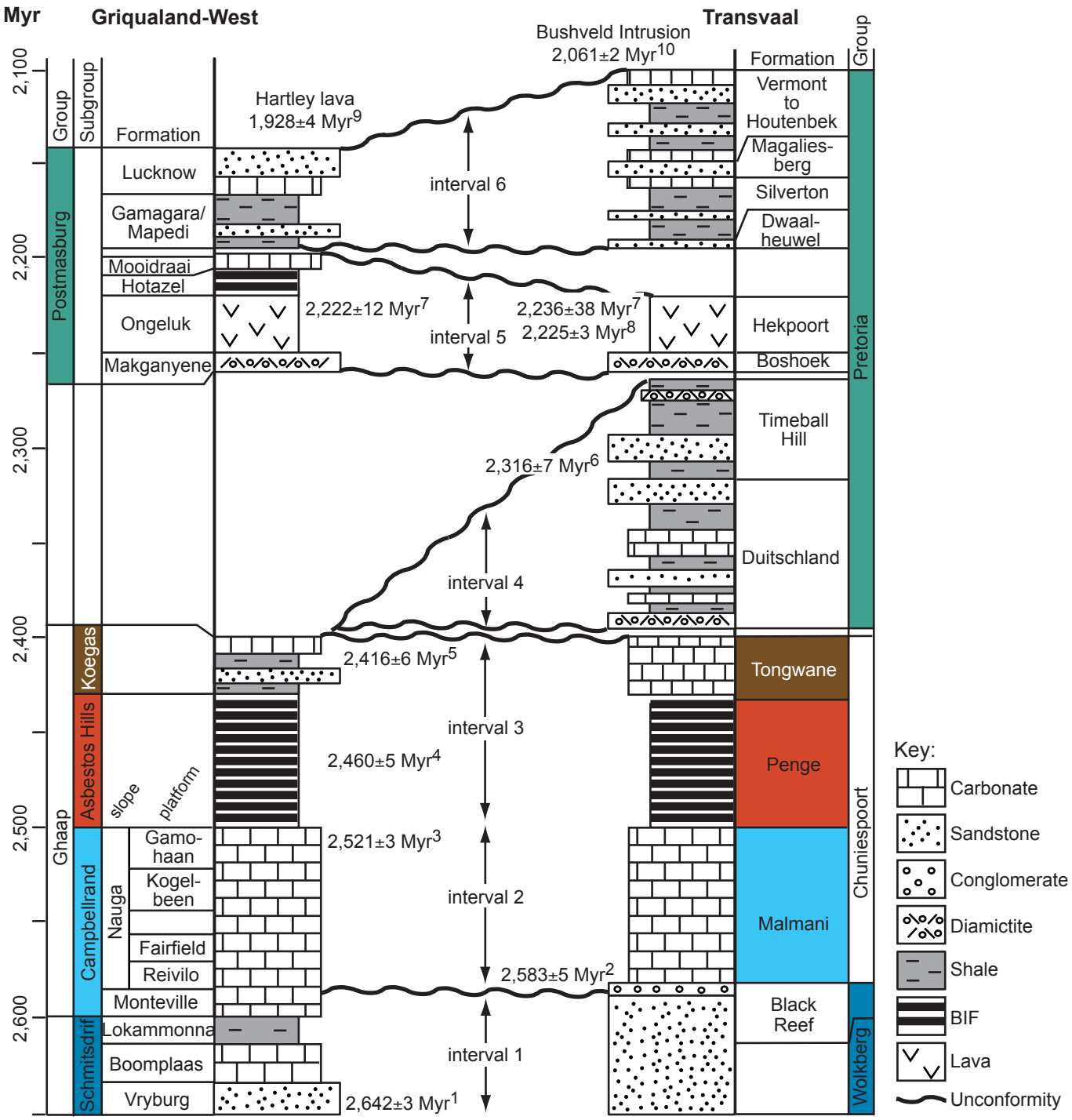

Figure DR1:Chronostratigraphy of the Transvaal Supergroup (based on Beukes et al., 2002; Dorland, 2004). The age dates are from: 1, (Walraven and Martini, 1995); 2, (Martin et al., 1998); 3, (Sumner and Bowring, 1996); 4, (Pickard, 2003); 5, (Gutzmer and Beukes, 1998); 6, (Hannah et al., 2004); 7, (Cornell et al., 1996); 8, (Dorland, 2004); 9, (Cornell et al., 1998); 10, (Walraven, 1997).

Section VEN
Lucknow Fm.
Farm Venn
S 28°04'21.9"
E 022°48'34.5"

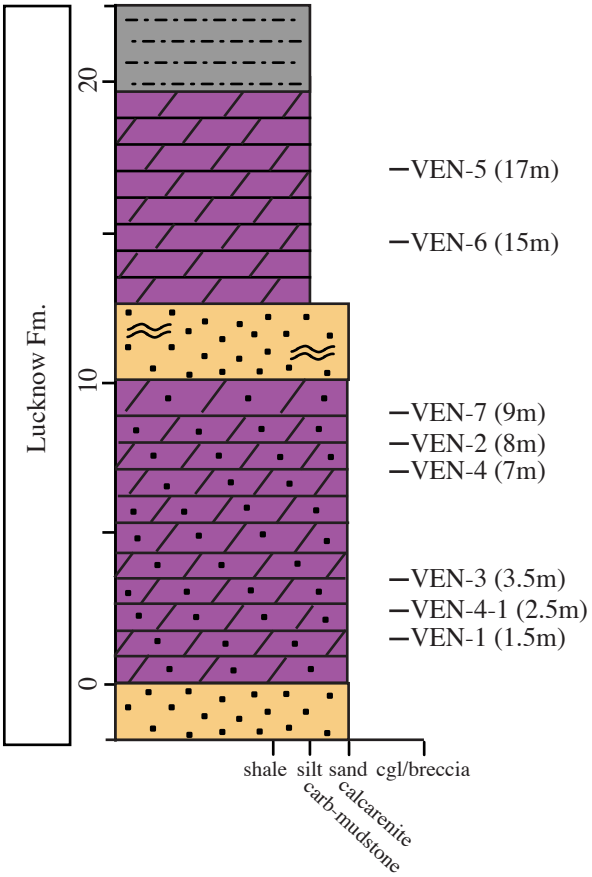

Section MOG
Silverton Fm.
Mogomane Hill
S 25°12'35.4"
E 025°46'32.9"

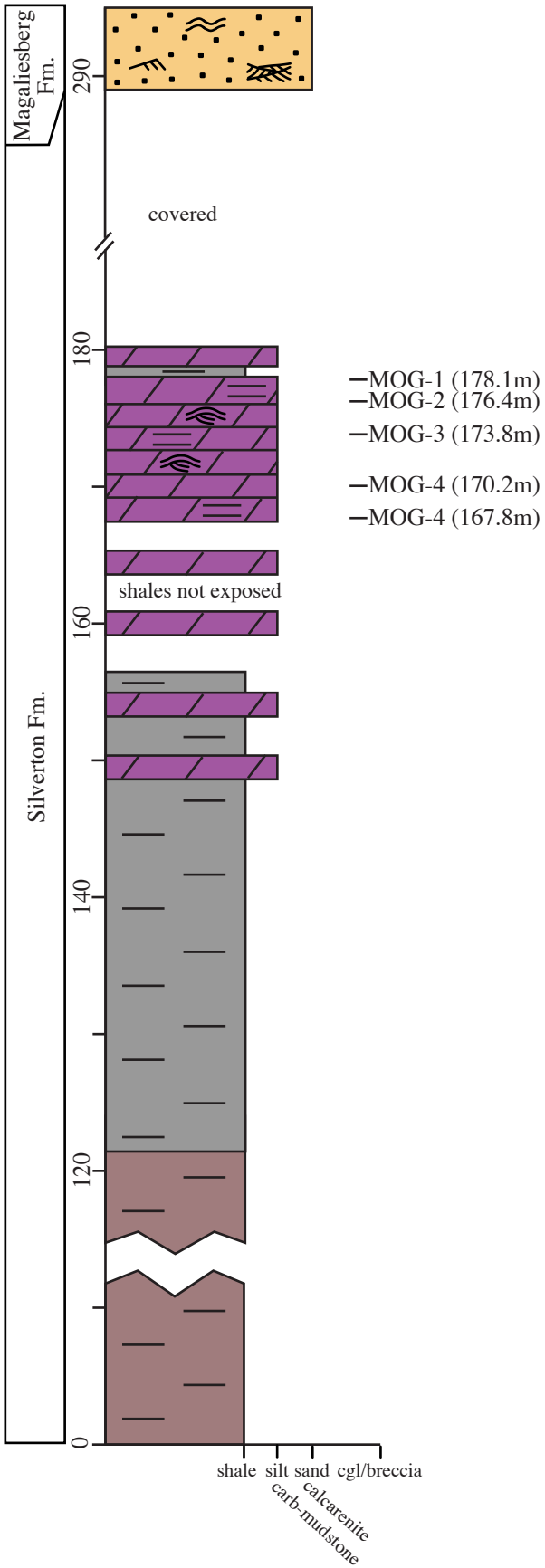

Core M10
Hotazel-Mooidraai Fm.
Farm Middelplaats (Anglo-American)

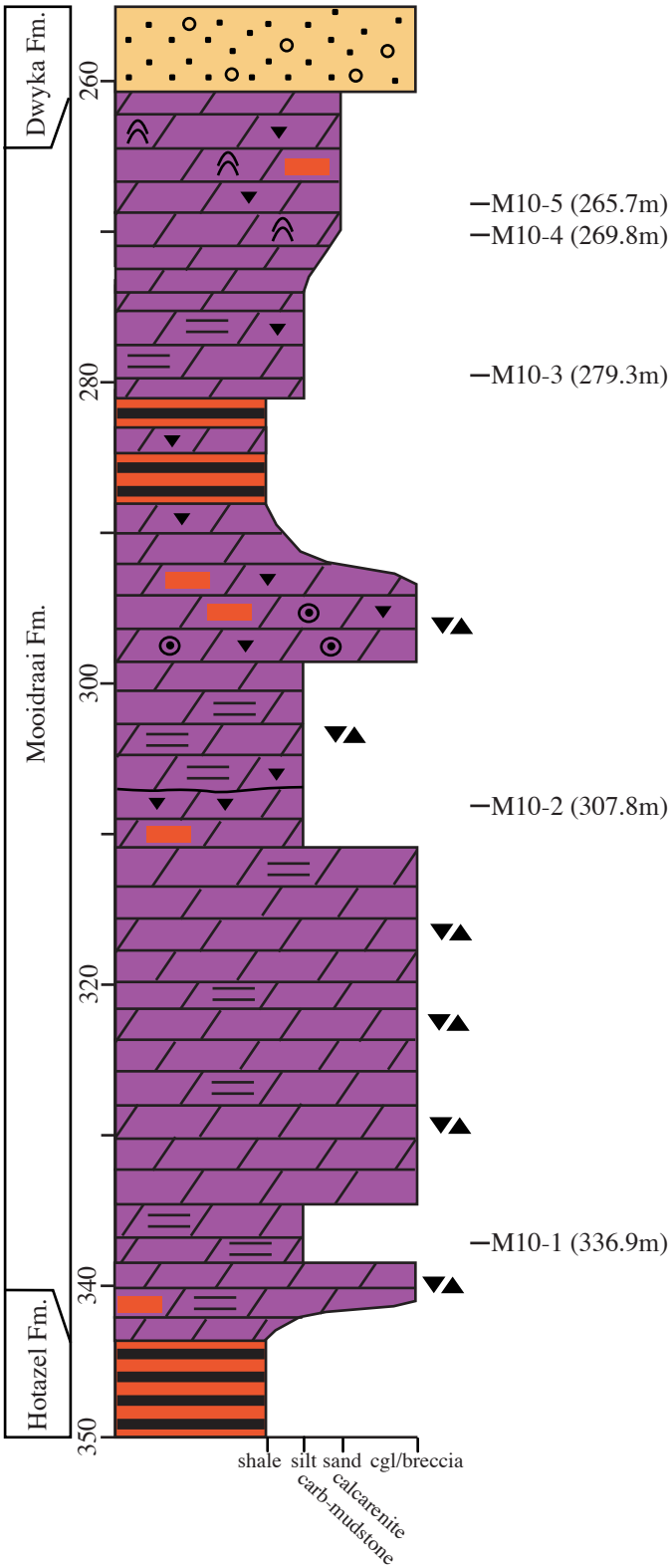

Section TON
Tongwane Fm.
Tongwane Gorge
S 24°10'43.6"
E 029°55'51.9"

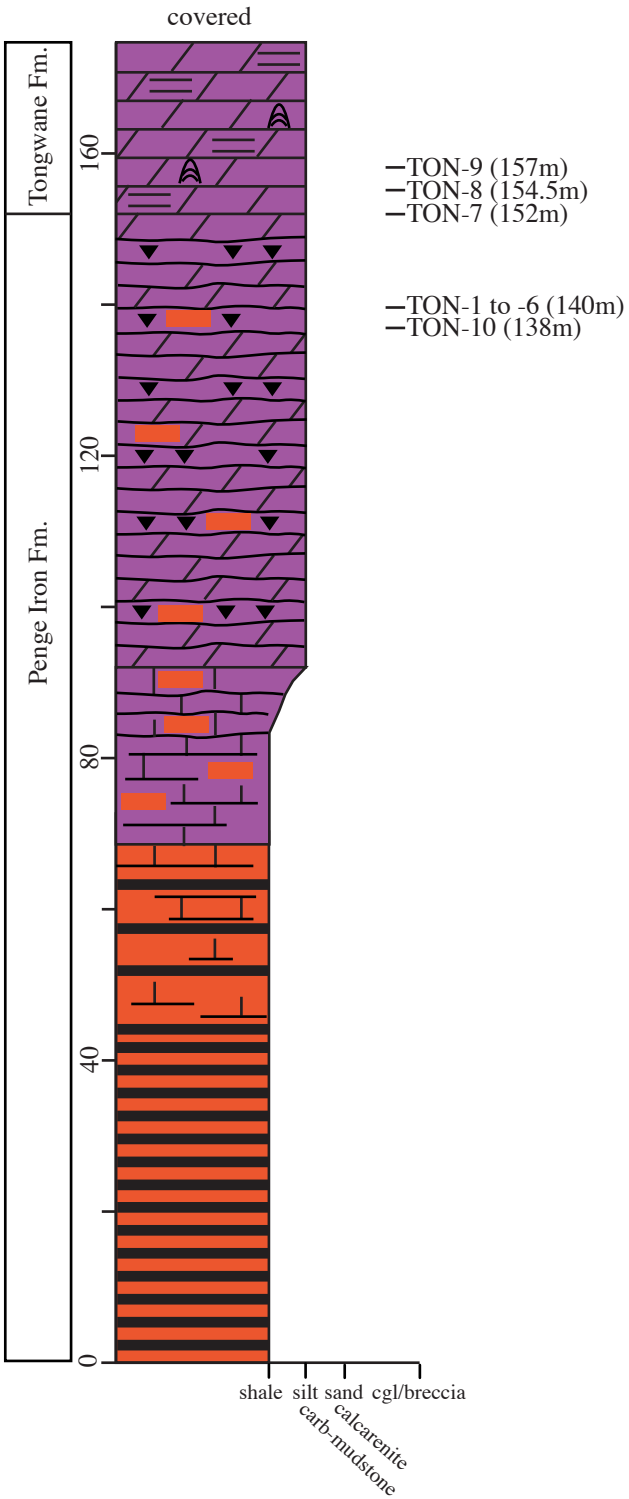

Section DUI
Duitschland Fm.
Farm Duitschland
S 24°17'44.0"
E 029°08'10.1"

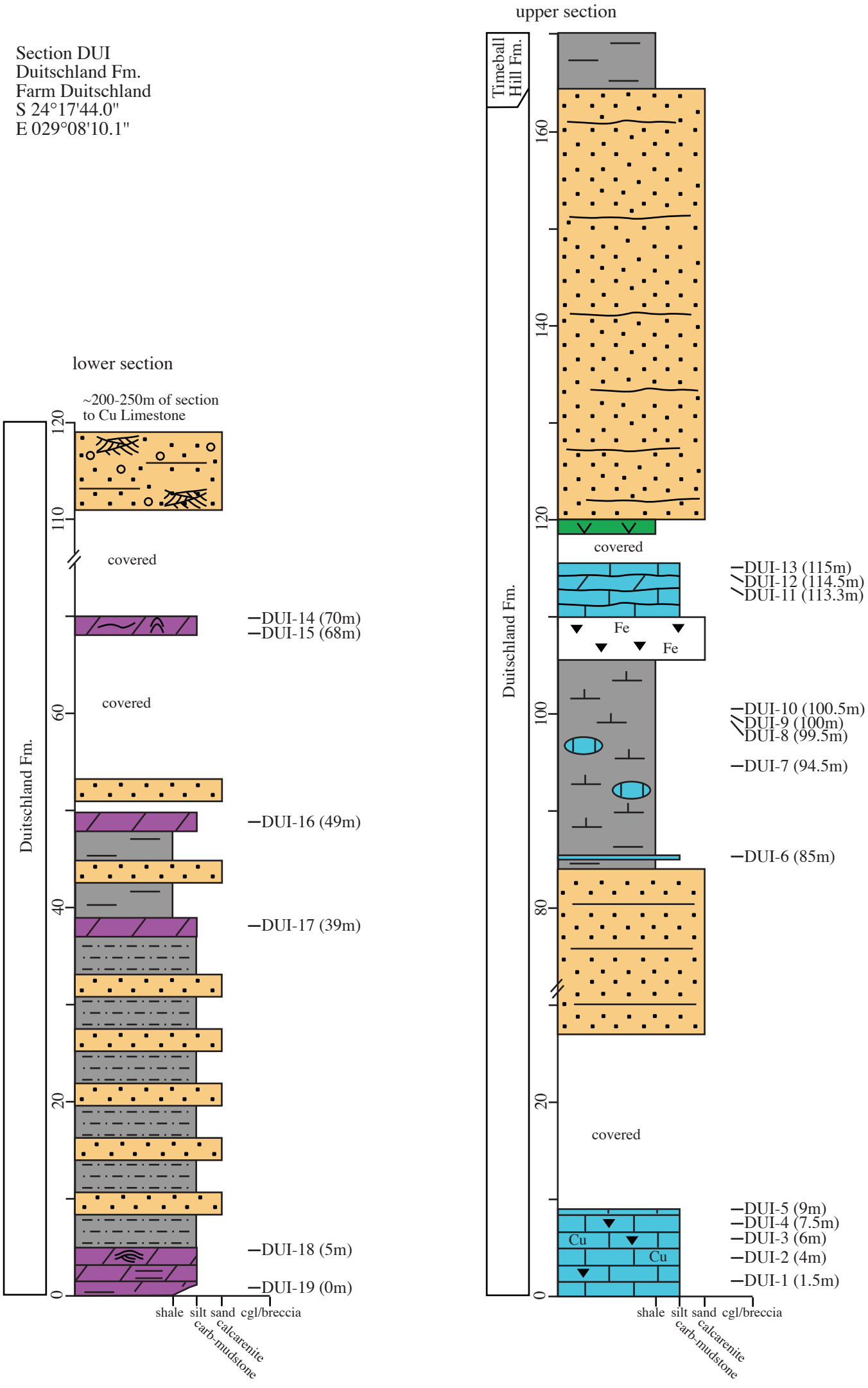

Section KOE
Koegas Subgp.
Farm Naragas
S 29°22'52.3"
E 022°34'58.1"

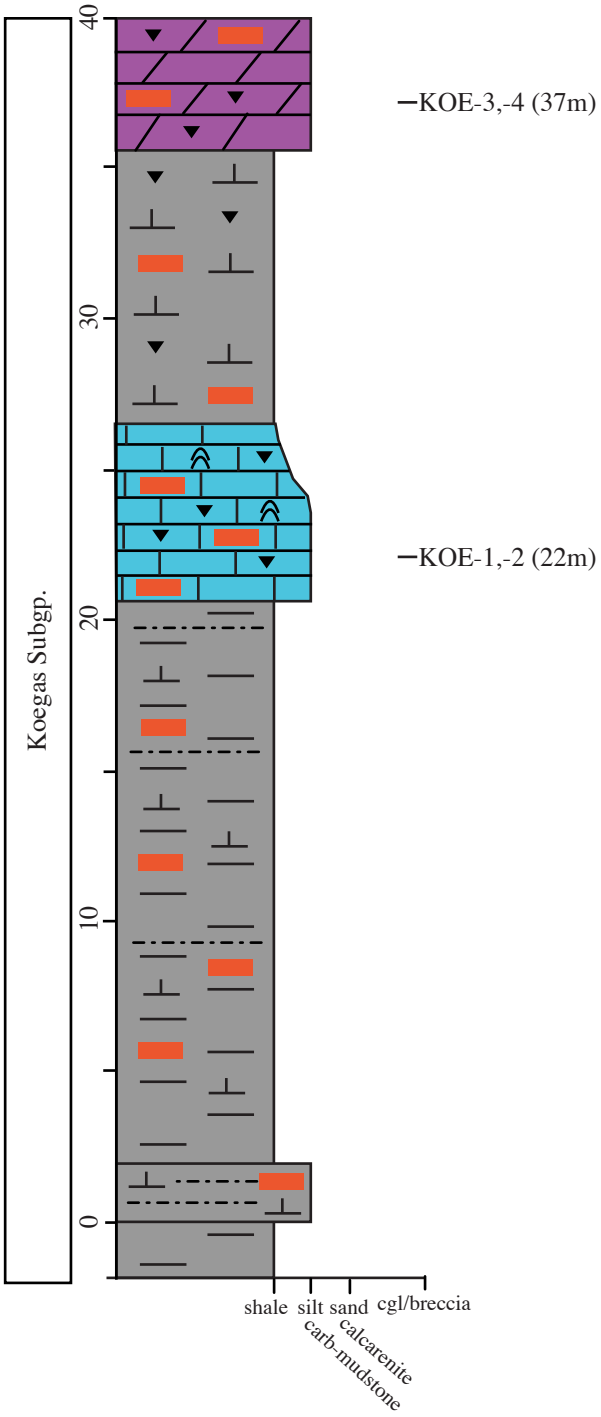

Section SAN
Koegas Subgp.
Farm Sandridge
S 28°49'21.7"
E 022°38'44.3"

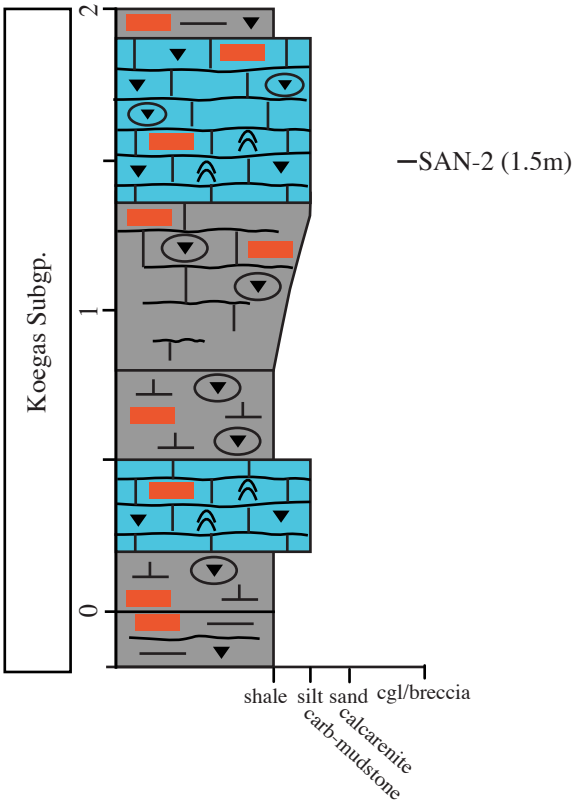

Section NAU (section 1)
Nauga Fm.
Farm Nauga
S 29°27'04.3"
E 022°20'50.9"

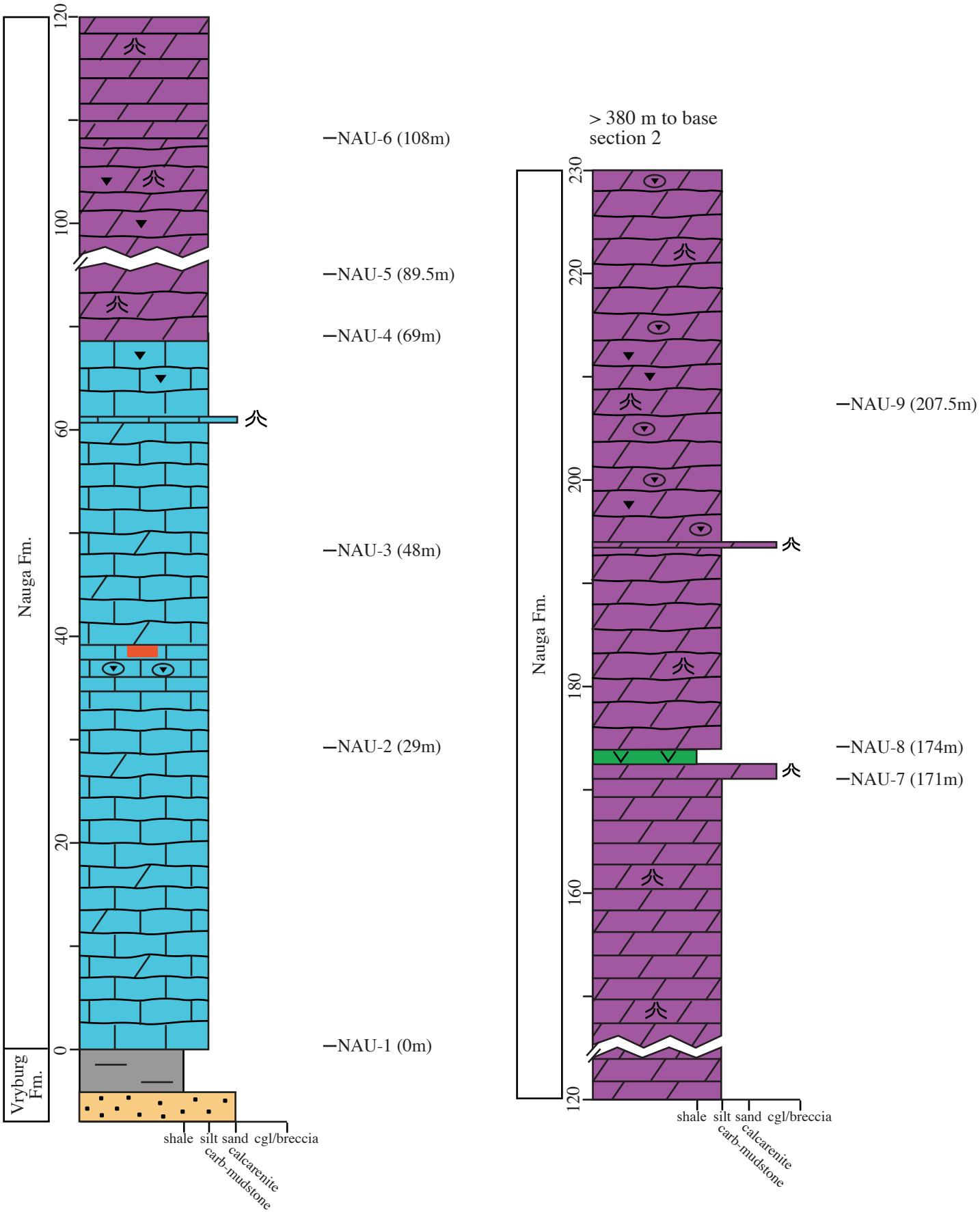

Section NAU (sections 2 and 3)
Nauga Fm.
Farm Nauga
S 29°27'04.3"
E 022°20'50.9"

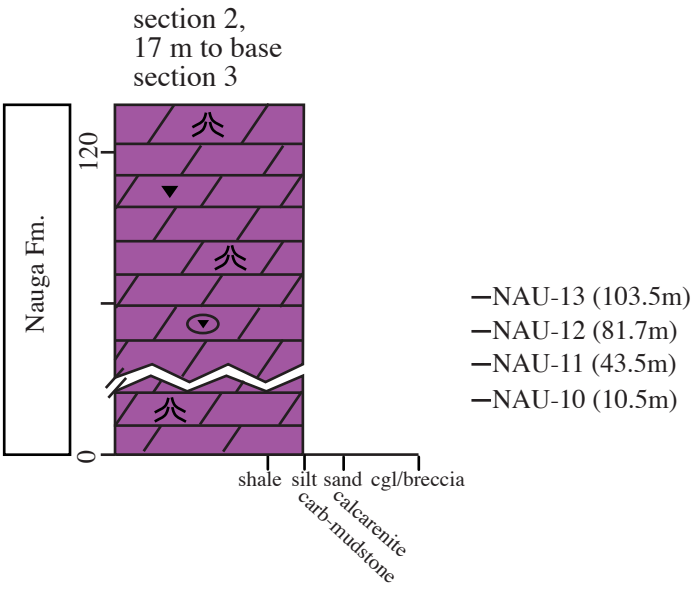

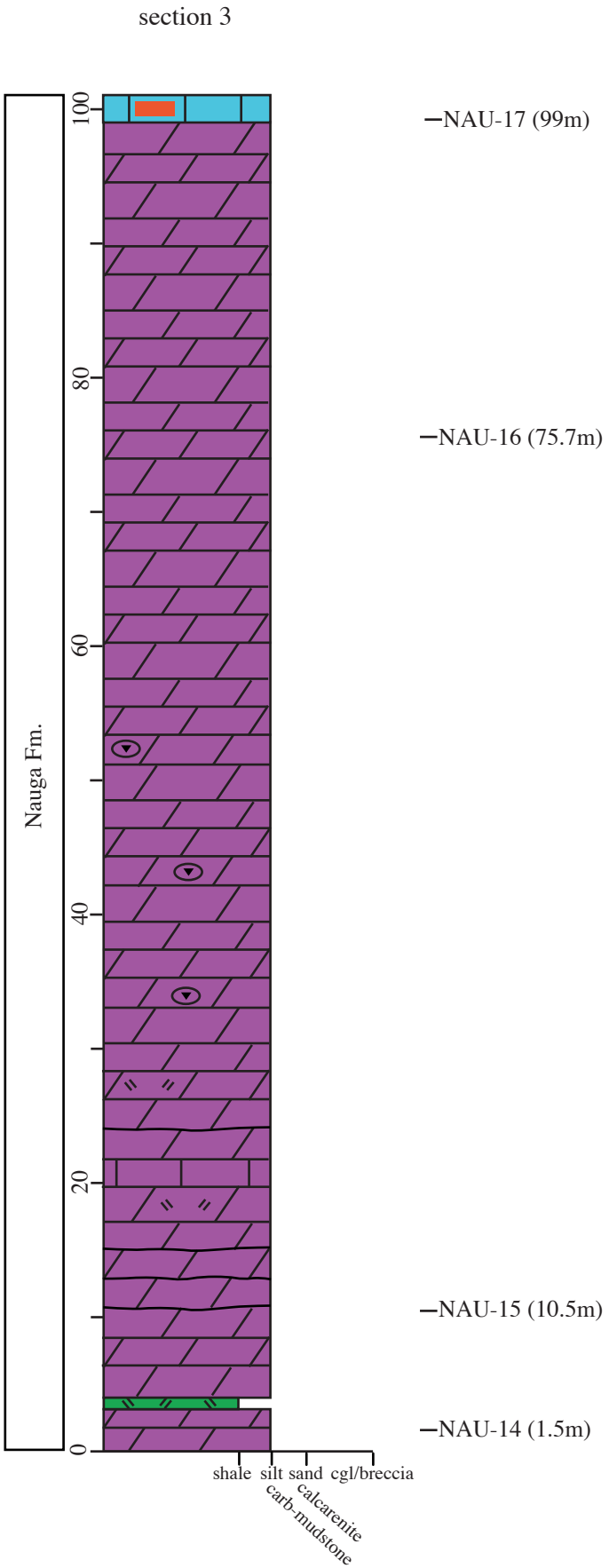

Section GLA
Gamohaan Fm.
Farm Gladstone
S 28°06'05.7"
E 023°34'45.3"

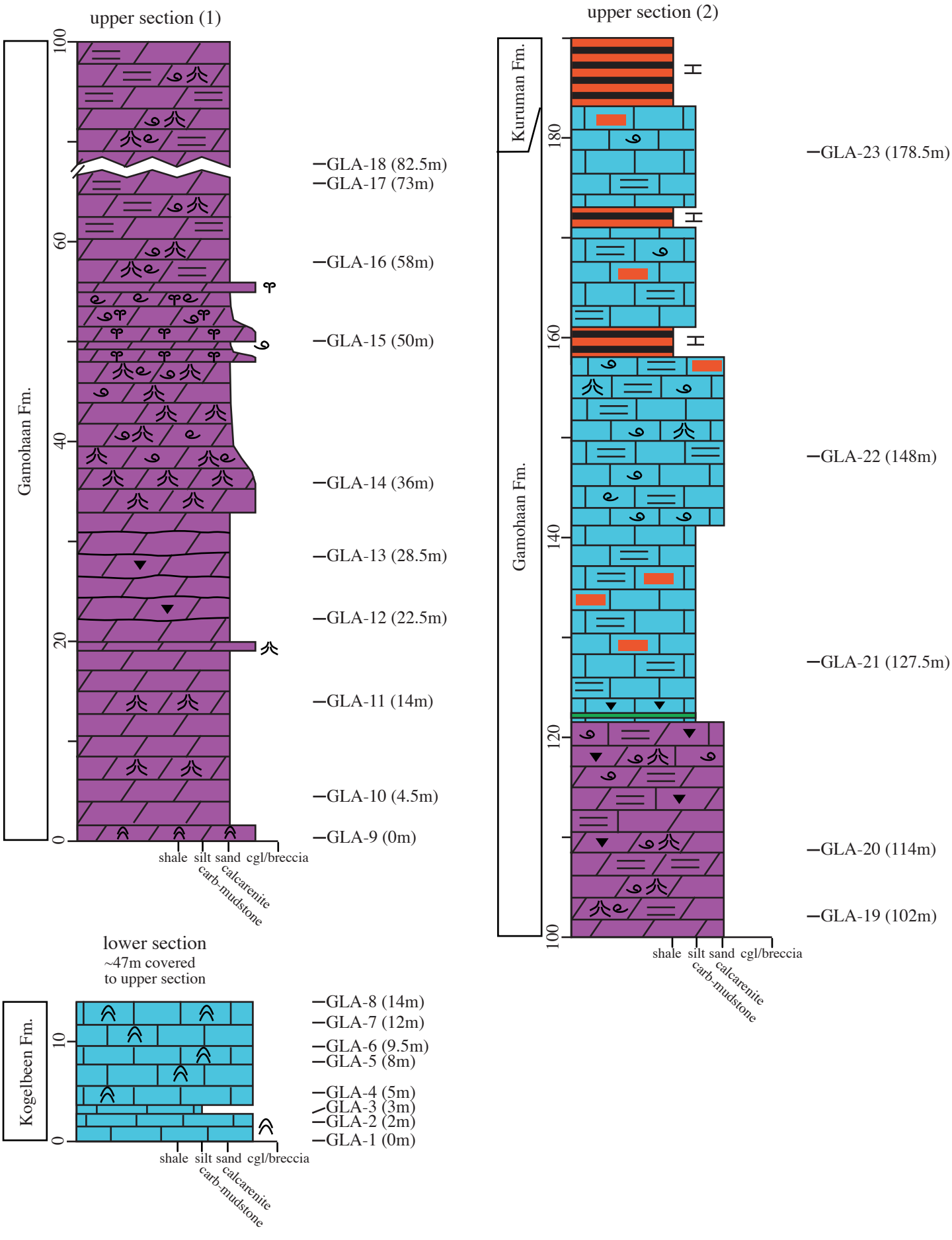

Section MON
Monteville Fm.
Farm Monteville
S 28°35'50.7"
E 023°58'01.2"

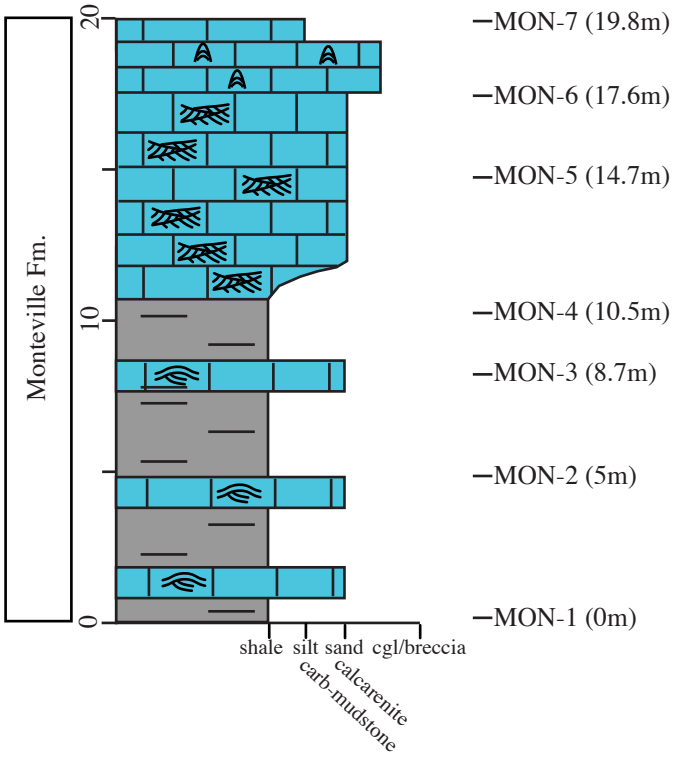

Section BAV
Reivilo Fm.
Farm Baviaanskrantz
S 28°35'16.9"
E 023°57'37.9'

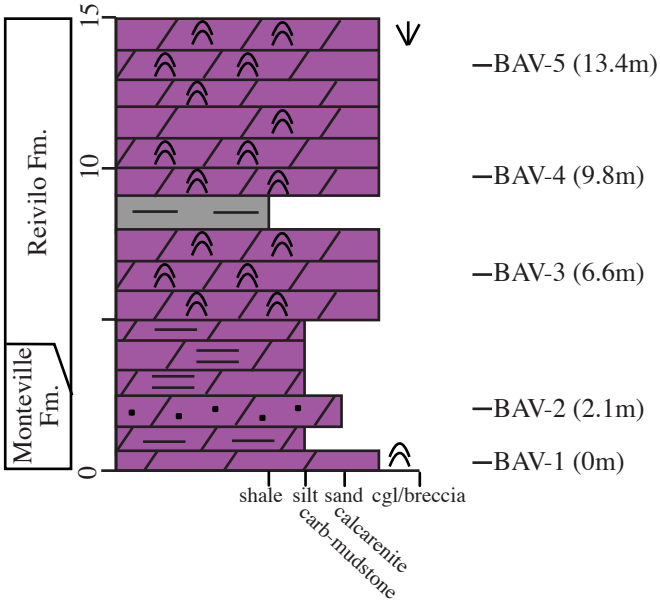

Section BOO
Boomplaas Fm.
Ulco-Schmitsdrif road
S 28°39'35.1"
E 024°01'44.1"

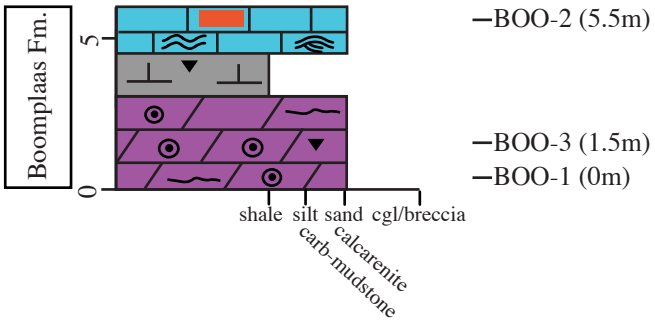

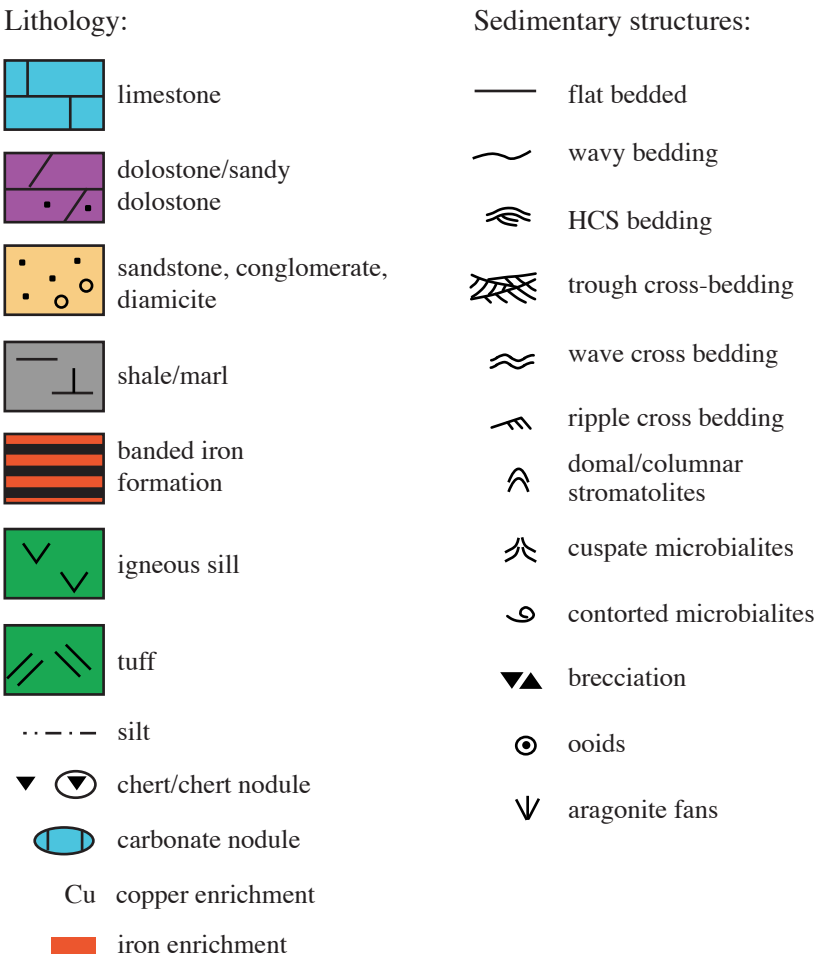

Figure DR2: The measured sections (in color) that show the position of the samples

Beukes, 2006). Shallow subtidal carbonates dominate over most of the platform(Fig. DR2); they pass to slope and basinal carbonates near the southwestern edge of the craton (Beukes, 1987; Sumner and Grotzinger, 2004). A major transgression caused drowning of the platform (Beukes, 1987; Beukes et al., 1990). The end of carbonate deposition is constrained by an age of 2,521±3Myr (Fig. DR1; Sumner and Bowring, 1996).

As a result of transgression, carbonates are overlain by deeper-marine shales and ultimately by open shelf banded iron formations (interval 3 in Fig. DR1). During subsequent regression, granular iron formations were deposited in epeiric sea, lagoonal and supratidal environments (Beukes, 1983, 1984). The transgressive-regressive sequence terminates with shelf and deltaic clastics, minor carbonates and iron formations of the Koegas Subgroup in the Griqualand-West basin (Fig. DR1; Beukes, 1983, 1984). In the Transvaal basin, iron formations pass conformably to Tongwane Formation shallow-water carbonates, which are likely equivalent to Koegas deposits (Swart, 1999). Iron formations are poorly dated, and the beginning of iron deposition has been estimated at ~2,500 Myr. The only available age constraint for the top of interval 3 comes from the Koegas Subgroup (2,516±6Myr; Gutzmer and Beukes, 1998). A basin wide unconformity developed after ~2,400 Myr (Fig. DR1).

Rocks with an age of ~2,400 to ~2,250 Myr are only known from the Transvaal basin (Fig. DR1), where an intracratonic basin formed during interval 4. Chronostratigraphic constraints are given by an age date of 2,316±6Myr (Hannah et al., 2004), and by correlation with global glaciogenic epochs (Bekker et al., 2001). Interval 4 includes diamictites, shallow-marine carbonates, and deltaic to shelf siliciclastics (Coetzee et al., 2006).

Another craton-wide unconformity developed after ~2,250 Gyr (Fig. DR1). Basal units of the overlying interval 5 can be correlated across the craton: the Makganyene-Boshoek diamictite (Polteau et al., 2006), gradually passing up section to sedimentary-volcanic rocks, dated between 2,222±12 Myr and 2,238±36 Myr (Cornell et al., 1996). A lateritic paleosoil profile developed craton-wide at the top of the volcanics (Beukes et al., 2002). In Griqualand-West, the volcanics are conformably overlain by banded iron and manganese formations of the Hotazel Formation

(Cairncross et al., 1997; Schneiderhan et al., 2006). The Hotazel Formation in turn passes up section to the shallow-marine carbonates of the Mooidraai Formation (Bau et al., 1999). These chemical sediments are not represented in the Transvaal basin (Fig. DR1 and DR2).

The last phase of Transvaal deposition (interval 6) started ~2,200 Myr with continental red beds (Fig. DR1; Beukes and Smit, 1987). Red beds pass up section to intracratonic shallow-marine carbonates and siliciclastics (Button and Vos, 1977; Eriksson et al., 2002; Swart, 1999). Carbonates have highly positive $\delta^{13}C$ values, indicating deposition during the 2,220-2,060 Myr Lomagundi carbon isotope excursion (Karhu and Holland, 1996; Swart, 1999). The Transvaal Supergroup is capped by a major angular unconformity, and overlain by volcanics in Griqualand West (1,928±4 Myr; Cornell et al., 1998; van Niekerk, 2006), and by the Bushveld intrusion in the Transvaal basin (2,061±2 Myr; Walraven, 1997) (Fig. DR1).

Stratigraphic unit, location	**Age**	**Facies description**	**Depositional environment**	**Reference**
Houtenbek Formation Rietvalley Farm for section: fig. 10 in Button and Vos (1977) S 25°42'15.4" E 029°57'41.4"	~2,070 Myr	Sandstone, limestone; sandstone with tabular cross bedding, flat bedding, current ripples, limestone with common domal and stratiform stromatolites with intraclastic breccias, mud cracks	Shallow subtidal and intertidal	Button and Vos (1977); Schreiber and Eriksson (1992)

Silverton Formation Mogomane Hill S 25°12'35.4" E 025°46'32.9"	~2,150 Myr	Shales passing up section to micritic dolostones with hummocky-cross stratification (HCS)	Open, storm-influenced shelf	Button (1973b; Eriksson et al. (2002)
Lucknow Formation Venn Farm S 28°04'21.9" E 022°48'34.5"	~2,150 Myr	Sandstones, siltstones, sandy dolostones; sandstones massive, cross bedded, with wave ripples, dolostones massive (locally stromatolitic)	Marginal marine, fluvio-deltaic sandstones, carbonate lagoons and sand/mud flats	Schröder et al. (2008), Swart (1999)
Mooidraai Formation	~2,200 Myr	Banded iron formations passing up section to Fe-bearing dolostones with chert; dolostones laminated, commonly brecciated, grainstone textures, at top stromatolitic	Deep subtidal (basinal), carbonates on shallow subtidal platform	Bau et al. (1999)
Duitschland Formation Duitschland Farm S 24°17'44.0"	~2,320 Myr	Interbedded shales, sandstones, dolostones, limestones; basal	Open shelf, storm- and wave-influenced	Swart (1999); Bekker et al. (2001)

E 029°08'10.1"		diamictite not included in section (~650 m below Cu limestone marker); carbonates with HCS and stromatolites, prominent Cu limestone marker, sandstones flat bedded and cross bedded		
Koegas Subgroup Naragas Farm S 29°22'52.3" E 022°34'58.1" Sandridge Farm S 28°49'21.7" E 022°38'44.3"	~2,430 Myr	Ferruginous mudstone (Fe lutite), cherty, with siltstone intercalations, meter-thick interbeds of ferruginous cherty limestone and dolostone; Fe lutite laminated, stromatolitic carbonates, some HCS	Open shelf around storm wave base, lagoons	Beukes (1978, 1983)
Tongwane Formation	~2,430 Myr	Banded iron formations passing up	Deep subtidal (basinal),	Swart (1999)

Tongwane Gorge S 24°10'43.6" E 029°55'51.9"		section to Fe-bearing dolostones with chert; dolostones massive and laminated, stromatolitic	carbonates on shallower platform?	
Nauga Formation Farm Nauga S 29°27'04.3" E 022°20'50.9"	~2,600-2,510 Myr	Limestone and dolostone, chert intercalations; massive, laminated fine-grained carbonates, ribbon rock, intercalations of fenestrate microbialites and contorted laminated mats	Slope of carbonate platform, below storm wave base	Beukes (1987); Sumner and Grotzinger (2004)
Kogelbeen-Gamohaan formations Farm Gladstone S 28°06'05.7" E 023°34'45.3"	~2,520-2,500 Myr	Kogelbeen: limestone; domal stromatolites Gamohaan: limestone and dolostone, passing to iron formation; grainstones and fenestrate microbialites, passing up section to	Kogelbeen: shallow subtidal, lagoonal; Gamohaan: deep subtidal to upper slope	Beukes (1987); Sumner (2002); Sumner and Grotzinger (2004)

		contorted laminated mats and shale		
Reivilo Formation Farm Baviaanskrantz S 28°35'16.9" E 023°57'37.9"	~2,590 Myr	Dolostones with interbedded shales; laminated dolostones pass up section to columnar and domal stromatolites Monteville-Reivilo sequence boundary marked by quartzose grainstone	Shallow subtidal to intertidal platform	Beukes (1987); Sumner (2002); Sumner and Grotzinger (2004)
Monteville Formation Farm Monteville S 28°35'50.7" E 023°58'01.2"	~2,600-2,590 Myr	Shallowing-upward shale-to-limestone cycles; shales rich in molar-tooth structures and interbedded with grainstones (HCS, wave ripples); limestones up section increasingly oolitic (bi-directional cross bedding) and stromatolitic, mud cracks	Shallowing from middle ramp (between storm and fair weather wave base) to inner ramp (stromatolites); peritidal at top	Beukes (1987); Sumner (2002); Sumner and Grotzinger (2004)

Boomplaas Formation Schmidtsdrif-Ulco road S 28°39'35.1", E 024°01'44.1"	~2.610-2,630 Myr	Limestone, dolostone, siltstones, shales; common ooids and subtidal stromatolites associated with platy breccias, HCS	Shallow to moderately deep subtidal	Beukes (1987); Sumner (2002)

Analytical Methods

The extraction of carbonate-associated sulfate involved a two-step procedure. Up to 1500g of rock powder was repeatedly leached with 10% NaCl-solution, prior to dissolution with 6M HCl, liberating CAS. This was either first precipitated as barium sulfate and subsequently converted to silver sulfide (Ag_2S) or directly reacted with Thode reagent (Thode et al., 1961), liberating H_2S that was captured as ZnS and subsequently converted to Ag_2S. Chromium-reducible sulfur was extracted from the mineral residue and precipitated as Ag_2S (Canfield et al., 1986). Barium sulfate and silver sulfide precipitates from sulfides were measured for their $\delta^{34}S$ values in Münster, Germany.

For multiple sulfur isotope analyses, silver sulfide was fluorinated to produce SF_6 (Johnston et al., 2005). All multiple sulfur isotope measurements were performed at the University of Maryland.

The $\delta^{34}S$ values are presented in the standard delta notation against V-CDT with an analytical reproducibility of $\leq$0.2‰ in both laboratories. The $\Delta^{33}S$ and $\Delta^{36}S$ values are defined as $\Delta^{33}S = 1000 \times (({}^{33}S/{}^{32}S)_{sample}/({}^{33}S/{}^{32}S)_{ref} - (({}^{34}S/{}^{32}S)_{sample}/({}^{34}S/{}^{32}S)_{ref})^{0.515})$, and $\Delta^{36}S = 1000 \times (({}^{36}S/{}^{32}S)_{sample}/({}^{36}S/{}^{32}S)_{ref} - (({}^{34}S/{}^{32}S)_{sample}/({}^{34}S/{}^{32}S)_{ref})^{1.9})$. We report these values against an assumed $\Delta^{33}S$ and

$\Delta^{36}S$ for V-CDT that yields $\delta^{34}S$, $\Delta^{33}S$ and $\Delta^{36}S$ values for IAEA S-1 of 0.3‰, 0.094‰, and 0.69‰. Uncertainties of $\Delta^{33}S$ and $\Delta^{36}S$ values by the SF_6 technique are on the order of 0.01 and 0.2‰.

Evaluation of data using non-steady state box models

We constructed a basic box model of the sulfur cycle in order to evaluate the transition from a non-mass dependent sulfur cycle to a sulfur cycle with higher oceanic sulfate concentrations and a strong influence of biological sulfate reduction (BSR). The structure of this model is given in Figure DR3 below.

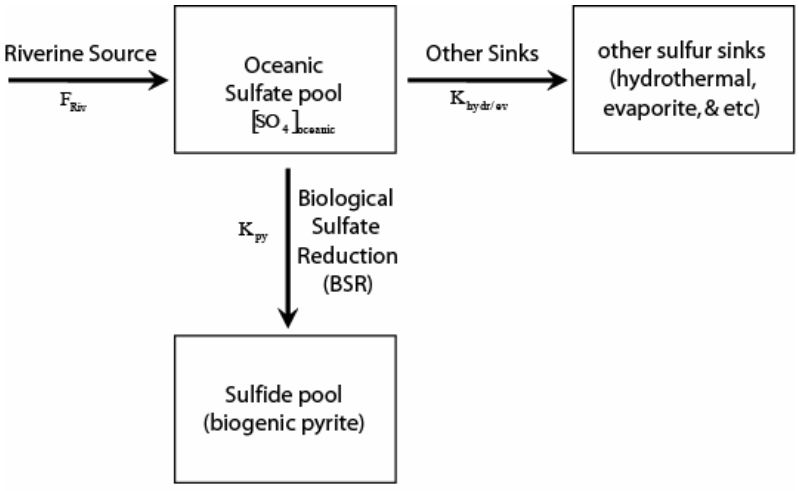

Figure DR3: Structure of sulfur cycle model used to evaluate whether the observations are consistent with non-steady state growth of a mass-dependent oceanic sulfate reservoir. Sulfur pools are labeled as boxes in this model and the transfer pathways are represented by the arrows. The flux of riverine sulfate is given by F_{riv}. The rate constants for BSR and other sulfate sinks are given by K_{py} and $K_{hydr/ev}$.

We make several simplifying assumptions about the rate constants that govern the sulfate sinks in this model in order to explore the response of this model to changes in the flux of riverine sulfate. The model assumes first order kinetic control on sulfate concentrations:

$$\frac{d[SO_4]_{oc}}{dt} = -(K_{py} + K_{hydr/ev})[SO_4]_{oc}, \quad (1a)$$

where K_{py} and $K_{hydr/ev}$ are the first order rate constant for the sinks of oceanic sulfate and $[SO_4]_{oc}$ is the concentration of sulfate in the oceanic pool. K_{py} is the rate constant describing the dependence of the sink attributable to biogenic pyrite formation and $K_{hydr/ev}$ is the rate constant describing the dependence of the sink attributable to other sulfate sinks which are principally hydrothermal and evaporitic sulfate sinks. First order kinetics assumes that the magnitude of both of these sulfate sinks is linearly related to sulfate concentration in the oceans.

For the balance of sulfate in the oceanic sulfate pool:

$$\frac{d[SO_4]_{oc}}{dt} = F_{in} - F_{out} = F_{riv} - (K_{py} + K_{hydr/ev}) * [SO_4]_{oc} \quad (1b)$$

This model can be solved for changes in the concentration of oceanic sulfate with time ($[SO_4]_{oc\_t}$) in terms of the initial oceanic sulfate concentration ($[SO_4]_{oc\_i}$) using:

$$[SO_4]_{oc\_t} = \frac{F_{riv}}{K_{py} + K_{hydr/ev}} - \left(\frac{F_{riv}}{K_{py} + K_{hydr/ev}} - [SO_4]_{oc\_i} \right) e^{-(K_{py} + K_{hydr/ev})t}, \quad (2a)$$

where t refers to time. We have initialized this model with an initial sulfate concentration of ~300 micromolar (~1% of present concentrations and solved to yield a 12 Myr residence time for sulfate – similar to that observed in the present-day oceans). At steady state, and assuming the first order rate constants that we have assumed, this condition is met when the source terms for sulfate (riverine) are 1% of present levels. We have then explored the response of the model to a tenfold increase in the flux of riverine sulfate with a mass-dependent isotopic composition.

We recognize that the sulfate sulfur produced by oxidative weathering immediately after the rise of oxygen, may have a mass-independent component, but we assume a mass-dependent composition for two reasons. The process of oxidative weathering will integrate the signal which will tend toward near zero values of $\Delta^{33}S$ and $\Delta^{36}S$ values of zero, and the rise of oxygen will also facilitate weathering of igneous, sulfide minerals which may have accumulated on the continents. The parameters used in this solution are given as:

Variable	Value
Initial $[SO_4]_{oceanic}$	0.3 mM* (300 μM)
$K_{hydr/ev}$	0.83e-8/yr†
K_{py}	7.49e-8/yr†
F_{riv}	3mM*/12e6yr
* These values can be converted to more commonly used quantities (e.g. moles or grams by multiplying by the amount of water in the oceanic pool and appropriate conversions). † These values are derived assuming a 12 Myr residence time for the oceanic sulfate pool.	

Incorporation of isotopes into the model

In order to explore the response of the model when isotopes are included we started with an initial isotopic composition for the oceanic pool of $\delta^{34}S$ = 17‰, $\Delta^{33}S$ = +2‰, and $\Delta^{36}S$ = -1.6‰. This composition was chosen to be slightly more ^{34}S and ^{33}S enriched than the non mass-dependent Duitschland data. We note that this composition is different from that observed in older Archean sediments (Ono et al.,

2003; Kaufman et al., 2007). A composition like this might result in cases where the sulfate pool carries an isotopic signature of sulfate reduction.

We then note that a solution can be obtained by solving this system for each of the isotopes and noting that the equations for the different isotopes of sulfur can be coupled using the fractionation factors for BSR given by:

$$^{34}\alpha_{BSR} = \frac{\left(^{34}S/^{34}S\right)_{py}}{\left(^{34}S/^{34}S\right)_{SO_4}}, \quad (4a)$$

$$^{33}\alpha_{BSR} = \left(^{34}\alpha_{BSR}\right)^{\lambda_3}, \text{ and} \quad (5a)$$

$$^{36}\alpha_{BSR} = \left(^{34}\alpha_{BSR}\right)^{\lambda_6}, \quad (6a)$$

where α is a fractionation factor and λ_3 and λ_6 are the exponents that relate the fractionation factors for the different isotopes. We couple the equations using a trace abundance approximation which assumes that K_{py} applies for ^{32}S and that $^{34}\alpha_{BSR}$* K_{py}, $^{33}\alpha_{BSR}$* K_{py}, and $^{36}\alpha_{BSR}$* K_{py} apply for ^{34}S, ^{33}S, and ^{36}S, respectively. The model assigns a dependence between the fractionation factors and sulfate concentration that is empirically derived from data presented in Habicht et al. (2002). Because of the dependence of the fractionation factor on concentration, we solved the model using numerical techniques, stepping the model forward with a 1 year time step for 200 million years. We checked the results of the model with the analytical solution using constant values for the fractionation factors.

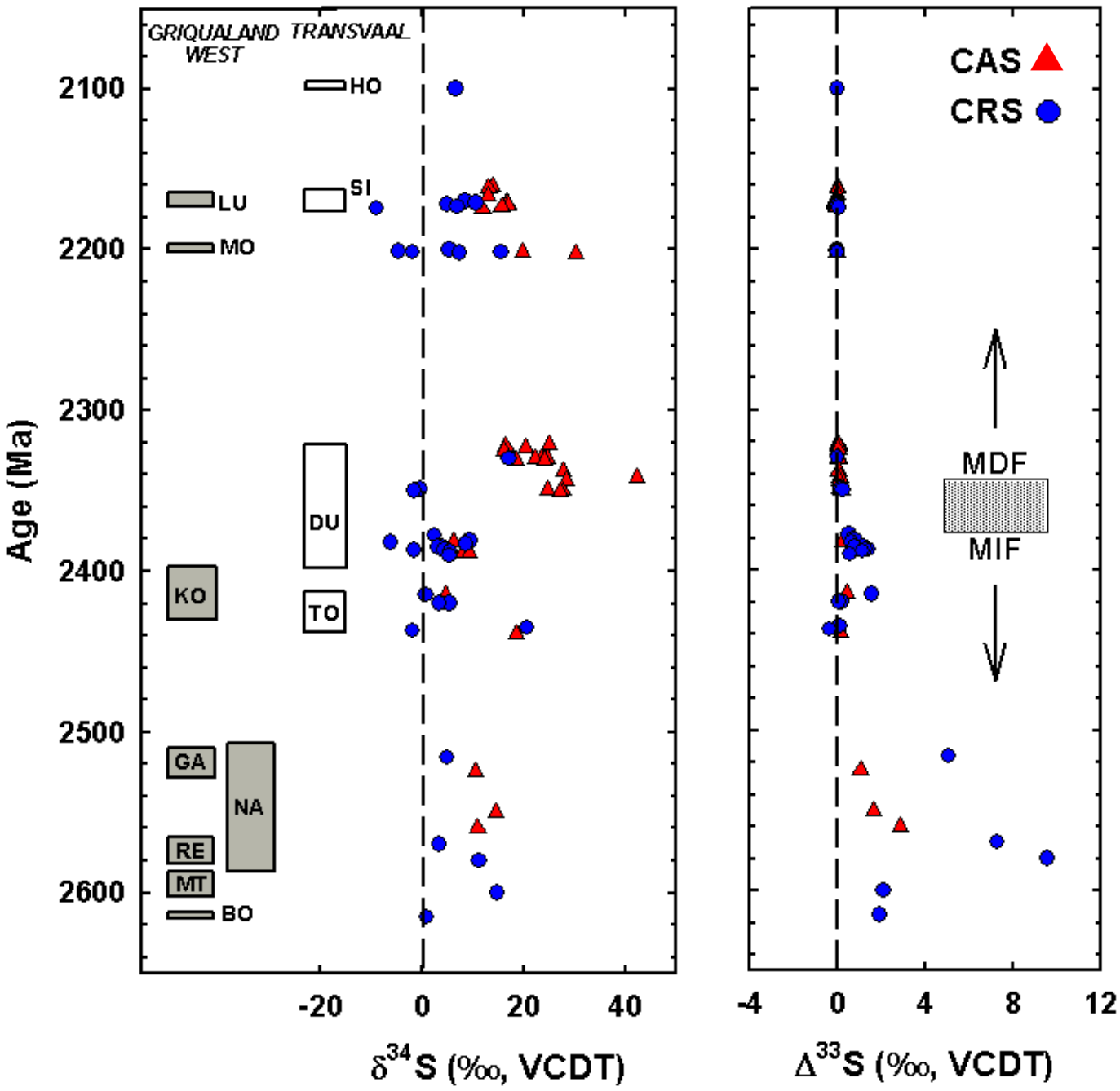

Figure DR4: Temporal variations in $\delta^{34}S_{CAS}$ and $\delta^{34}S_{CRS}$ (left panel) and $\Delta^{33}S$ values (right panel) for carbonates from the Transvaal Supergroup. A transitional band is shown to indicate the decline in non-mass dependent fractionation (MIF) likely associated with the onset of the GOE. MDF = Mass-dependent fractionation. CAS=Carbonate-associated sulfate, CRS=Chromium-reducible sulfur. HO = Houtenbek; SI = Silverton, LU = Lucknow, MO = Moodraai, DU = Duitschland, KO = Koegas Subgroup, TO = Tongwane, NA = Nauga, GA = Gamohaan, RE = Reivilo, MT = Monteville, BO = Boomplaas.

Comparison of model results with observations

Sulfur isotope compositions of carbonate-associated sulfate (CAS) and chromium-reducible sulfur (CRS) throughout the Transvaal Supergroup are presented in Figure DR4. Solutions to our model calculations are given in Figures DR5 and DR6 and indicate that the model can capture several broad features that are present in the data. The inclusion of a concentration-dependent fractionation factor in the model yields generally smaller fractionations between sulfate and sulfide when MIF is present and a divergence in values for $\delta^{34}S$ and $\Delta^{36}S$ from $\Delta^{33}S$ of sulfate and sulfide as the system evolves from MIF to MDF and higher SO_4 concentration. There are features of the data that the model does not reproduce such as a trajectory for the data and this is taken as an indication that the natural system is more complex than the model. The model also does not reproduce the scatter in the CRS data, the positive ^{34}S of many of the chrome reducible sulfur, and the strongly positive $\delta^{34}S$ of one CAS Duitschland Formation sample. We suggest that these features indicate that a more complex scenario may be necessary to reproduce the data, possibly one with non-conservative behavior of sulfate in the oceanic sulfate pool (geographic variability) such as has been suggested before (Kaufman et al., 2007; Logan et al., 1995; Johnston et al., 2006).

Insight from free parameters

While some of the constraints on the model were chosen to be consistent with independent criteria other constraints were chosen to fit the model to the data. These are considered to be free parameters and include the initial composition of the sulfate and the fraction of pyrite burial (assumed to be 90% of the total sink (K_{py}/(K_{py} +

$K_{hydr/ev}$)). The choice of these values may carry implications for evaluation of the Duitschland Formation S isotope record.

The initial composition of the sulfate pool chosen in the model has a positive rather than negative $\Delta^{33}S$ values in contrast to previous suggestions (Farquhar et al.2000, 2003, 2005). The positive $\Delta^{33}S$ may be an important feature of the initial oxidation of emergent sulfide-bearing rocks, or it may represent some other process that remains to be identified.

The fraction of pyrite burial (90% of the total sulfate sink) is high. We think this value may imply that the model is too simple and that a more complex model is required.

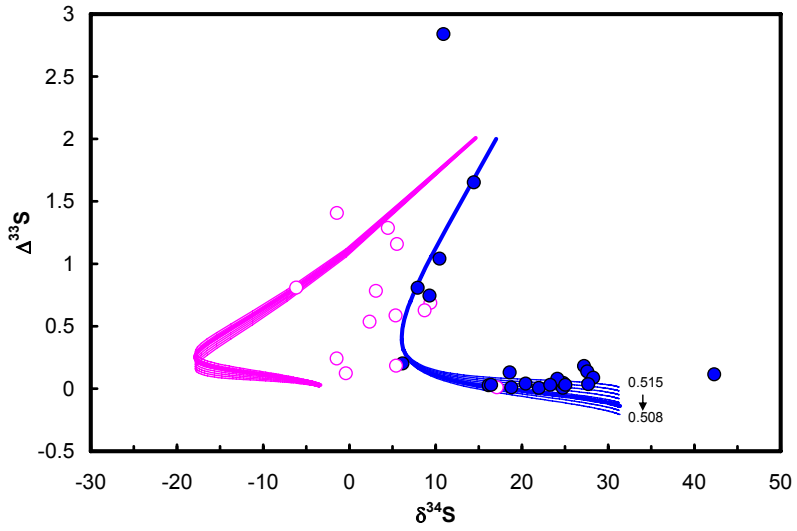

Figure DR5: Plot of $\Delta^{33}S$ vs $\delta^{34}S$ with model results (lines) and data from Duitschland and Malmani formations on Duitschland Farm. Filled blue symbols are the sulfate and unfilled purple symbols are the Chrome-reducible sulfide. The thin lines are calculated for sulfate and sulfide using a variety of theoretical exponents for predictions of sulfate reduction extending from 0.515 to 0.508 for λ_3. The two thick lines are calculated for sulfate and sulfide using measured exponents for sulfate reduction from Johnston et al. 2007.

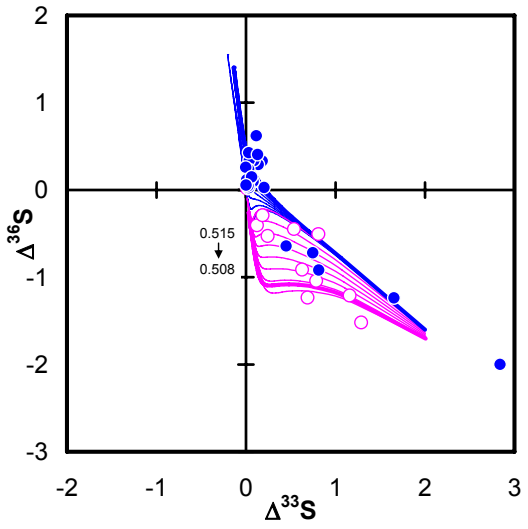

Figure DR6: Plot of $\Delta^{36}S$ vs $\Delta^{36}S$ with model results (lines) and data from Duitschland and Malmani formations on Duitschland Farm. Filled blue symbols are the sulfate and unfilled purple symbols are the Chrome-reducible sulfide. The thin lines are calculated for sulfate and sulfide using a variety of theoretical exponents for predictions of sulfate reduction extending from 0.515 to 0.508 for λ_3. The two thick lines are calculated for sulfate and sulfide using measured exponents for sulfate reduction from Johnston et al. (2007).

Assuming the catabolism of aerobic respirer is limited only by O_2 (Jin and Bethke, 2005), just as it might have occurred right before the oxygen rise in Precambrian time, the rates (r) of aerobic respiration can be described according to the Monod equation (Eq 7) $r = k*[X]*[O_2]/([O_2]+KA)$ where k is the rate constant, [X] is biomass concentration, $[O_2]$ is dissolved oxygen concentration, and KA is half-saturation constant.

Concurrently with respiration, microorganisms synthesize their biomass, increasing [X], (Eq 8) $d[X]/dt = Y*r\ D*[X]$ where Y is the growth yield and D is the decay constant. Note that in order to survive in the environment, the growth rate must be maintained positive, i.e., $d[X]/dt > 0$.

Based on our current understanding of modern aerobic respirer, we can take

average values of k = 1.0E6 mol/g/sec KA = 1.0E-8 mol/liter

Y = 15 g/mol D = 1.0E-7 1/sec.

These values are based on laboratory measurements, not any assumptions. Substituting these values into the equations and note that d[X]/dt > 0, we can calculate a minimum value required by aerobic microbes to evolve on Earth: $[O_2]$min = 6.7E-11 mol/liter, which is about 8.8E-8 atm of O_2.

If the constrains of electron donors, such as acetate and H_2 (two dominant substrates in the environment), are considered, the minimum value may increase about 10 to 100 fold, i.e., 10^{-6} to 10^{-5} atm.

REFERENCES CITED

Bau, M., Romer, R. L., Lüders, V. and Beukes, N. J., 1999, Pb, O, and C isotopes in silicified Mooidraai dolomite (Transvaal Supergroup, South Africa): implications for the composition of Paleoproterozoic seawater and `dating' the increase of oxygen in the Precambrian atmosphere: Earth and Planetary Science Letters, v. 174, p. 43-57.

Bekker, A., Kaufman, A. J., Karhu, J. A., Beukes, N. J., Swart, Q. D., Coetzee, L. L. and Eriksson, K. A., 2001, Chemostratigraphy of the Paleoproterozoic Duitschland Formation, South Africa: Implications for coupled climate change and carbon cycling: American Journal of Science, v. 301, p. 261-285.

Beukes, N. J., Dorland, H. C., Gutzmer, J., Nedachi, M. and Ohmoto, H., 2002, Tropical laterites, life on land, and the history of atmospheric oxygen in the Paleoproterozoic: Geology, v. 30, p. 491-494.

Beukes, N. J., 1978, Die karbonaatgesteentes en ysterformasies van die Ghaap-Groep van die Transvaal-Supergroep in Noord-Kaapland. Ph.D. Thesis, Rand

Afrikaans University, Johannesburg, 580 p.

Beukes, N. J., 1979, Litostratigrafiese onderverdeling van die Schmitsdrif-subgroep van die Ghaap-groep in noord-Kaapland: Transactions of the Geological Society of South Africa, v. 82, p. 313-327.

Beukes, N. J., 1983, Palaeoenvironmental setting of iron-formations in the depositional basin of the Transvaal Supergroup, South Africa. In: Trendall, A.F. and Morris, R.C. (Trendall, A.F. and Morris, R. C. (Trendall, A.F. and Morris, R. C.s) Iron formation: facts and problems. Developments in Precambrian Geology, v. 6, Elsevier, Amsterdam, p.131-209.

Beukes, N. J., 1984, Sedimentology of the Kuruman and Griquatown iron-formations, Transvaal Supergroup, Griqualand West, South Africa: Precambrian Research, v. 24, p. 47-84.

Beukes, N. J., 1987, Facies relations, depositional environments and diagenesis in a major Early Proterozoic stromatolitic carbonate platform to basin sequence, Campbellrand Subgroup, Transvaal Supergroup, Southern Africa: Sedimentary Geology, v. 54, p.1-46.

Beukes, N. J., Klein, C., Kaufman, A. J. and Hayes, J. M., 1990, Carbonate petrography, kerogen distribution, and carbon and oxygen isotope variations in an Early Proterozoic transition from limestone to iron-formation deposition, Transvaal Supergroup, South Africa: Economic Geology, v. 85, p. 663-690.

Beukes, N. J. and Smit, C. A., 1987, New evidence for thrust faulting in Griqualand West, South Africa: implications for stratigraphy and the age of red beds. South African Journal of Geology 90, 378-394.

Button, A., 1973a, The depositional history of the Wolkberg proto-basin, Transvaal: Transactions of the Geological Society of South Africa, v. 76, p.15-25.

Button, A., 1973b, A regional study of the stratigraphy and development of the

Transvaal basin in the eastern and northeastern Transvaal. PhD, University of the Witwatersrand, Johannesburg, 352 p.

Button, A. and Vos, R. G., 1977, Subtidal and intertidal clastic and carbonate sedimentation in a macrotidal environment: an example from the Lower Proterozoic of South Africa: Sedimentary Geology, v. 18, p.175-200.

Canfield, D.E., Raiswell, R., Westrich, J., Reaves, C., and Berner, R.A., 1986, The use of chromium reduction in the analysis of inorganic sulfur in sediments and shales: Chemical Geology, v. 54, p. 149–155, doi: 10.1016/0009-2541(86)90078-1.

Cairncross, B. C., Beukes, N. J. and Gutzmer, J., 1997, The Manganese Adventure: The South African Manganese Fields. Associated Ore and Metal Corporation, Johannesburg.

Coetzee, L. L., Beukes, N.J., Gutzmer, J. and Kakegawa, T., 2006, Links of organic carbon cycling and burial to depositional depth gradients and establishment of a snowball Earth at 2.3 Ga. Evidence from the Timeball Hill Formation, Transvaal Supergroup, South Africa: South African Journal of Geology, v. 109, p. 109-122.

Cornell, D. H., Armstrong, R.A. and Walraven, F., 1998, Geochronology of the Proterozoic Hartley Basalt Formation, South Africa: constraints on the Kheis tectogenesis and the Kaapvaal Craton's earliest Wilson Cycle: Journal of African Earth Sciences, v. 26, p. 5-27.

Cornell, D. H., Schütte, S. S. and Eglington, B. L., 1996, The Ongeluk basaltic andesite formation in Griqualand West, South Africa: submarine alteration in a 2222 Ma Proterozoic sea: Precambrian Research, v. 79, p. 101-123.

Dorland, H. C., 2004, Provenance ages and timing of sedimentation of selected Neoarchean and Paleoproterozoic successions on the Kaapvaal Craton. Ph.D.

Thesis, Rand Afrikaans University, Johannesburg, 326 p.

Eriksson, P. G., Altermann, W., Eberhardt, L., Arend-Heidbrinck, S. and Bumby, A.J., 2002, Palaeoproterozoic epeiric sea palaeoenvironments: the Silverton Formation (Pretoria Group, Transvaal Supergroup), South Africa. In: Altermann, W. and Corcoran, P.L. (eds) Precambrian Sedimentary Environments: a modern approach to ancient depositional systems: Special Publication of the International Association of Sedimentologists, v. 33, p. 351-367.

Eriksson, K. A., Simpson, E.L., Master, S. and Henry, G., 2005, Neoarchean (c. 2.58 Ga) halite casts: implications for palaeoceanic chemistry: Journal of the Geological Society, London, v. 162, p. 789-799.

Farquhar, J., Bao, H. M. and Thiemens, M., 2000, Atmospheric influence of Earth's earliest sulfur cycle: Science, v. 289, p. 756-758.

Farquhar, J. and Wing, B. A., 2003, Multiple sulfur isotopes and the evolution of the atmosphere: Earth and Planetary Science Letters, v. 213, p. 1–13.

Farquhar, J. and Wing, B. A. , 2005, in Mineral Deposits and Earth Evolution (eds McDonald, I., Boyce, A. J., Butler, I. B., Herrington, R. J. and Polya, D. A.) 167–177 (Spec. Publ. 248,Geological Society, London.

Gutzmer, J. and Beukes, N. J., 1998, High grade manganese ores in the Kalahari manganese field: Characterisation and dating of ore forming events. Unpublished Report, Rand Afrikaans University, Johannesburg, 221 p.

Habicht, K. S., Gade, M., Thamdrup, B., Berg, P. and Canfield, D. E., 2002, A calibration of sulfate levels in the Archean ocean: Science, v. 298, p. 2372-2374.

Hannah, J. L., Bekker, A., Stein, H. J., Markey, R. J. and Holland, H. D., 2004, Primitive Os and 2316 Ma age for marine shale: implications for

Paleoproterozoic glacial events and the rise of atmospheric oxygen: Earth and Planetary Science Letters, v. 225, p. 43-52.

Jin, Q., Bethke, C. M., 2005, Predicting the rate of microbial respiration in geochemical environments: Geochimica et Cosmochimica Acta, v. 69, p. 1133-1143.

Johnston, D. T., Wing, B. A., Farquhar, J., Kaufman, A. J., Strauss, H., Lyons, T. W., Kah, L. C., and Canfield, D. E., 2005, Active microbial sulfur disproportionation in the Mesoproterozoic: Science, v. 310, p.1477-1479.

Johnston, D. T. et al., 2006, Evolution of the oceanic sulphur cycle at the end of the Paleoproterozoic: Geochimica et Cosmochimica Acta, v. 70, p. 5723-5739.

Johnston, D. T., Farquhar, J. and Canfield, D. E., 2007, Sulfur isotope insights into microbial sulfate reduction: When microbes meet models: Geochimica et Cosmochimica Acta, v. 71, p. 3929-3947.

Karhu, J. A. and Holland, H. D., 1996, Carbon isotopes and the rise of atmospheric oxygen: Geology, v. 24, p. 867-870.

Kaufman, A. J., Johnston, D. T., Farquhar, J., Masterson, A., Lyons, T. W., Bates, S., Anbar, A. D., Arnold, G. L., Garvin, J. and Buick, R., 2007, Late Archean Biospheric Oxygenation and Atmospheric Evolution: Science, v. 317, p. 1900-1903.

Logan, G. A., Hayes, J. M., Hieshima, G. B. and Summons, R. E., 1995, Terminal Proterozoic reorganization of biogeochemical cycles: Nature, v. 376, p. 53-56.

Martin, D. M., Clendenin, C. W., Krapez, B. and McNaughton, N. J., 1998, Tectonic and geochronological constraints on late Archaean and Palaeoproterozoic stratigraphic correlation within and between the Kaapvaal and Pilbara cratons: Journal of the Geological Society, London, v. 155, p. 311-322.

Ono, S., Eigenbrode, J. L., Pavlov, A. A., Kharecha, P., Rumble, D. III, Kasting, J. F.

and Freeman, K. H., 2003, New insights into Archean sulfur cycle from mass-independent sulfur isotope records from the Hamersley Basin, Australia: Earth and Planetary Science Letters, v. 213, p.15-30.

Pickard, A. L., 2003, SHRIMP U–Pb zircon ages for the Palaeoproterozoic Kuruman Iron Formation, Northern Cape Province, South Africa: evidence for simultaneous BIF deposition on Kaapvaal and Pilbara Cratons: Precambrian Research, v.125, p. 275-315.

Polteau, S., Moore, J. M. and Tsikos, H., 2006, The geology and geochemistry of the Palaeoproterozoic Makganyene diamictite: Precambrian Research, v. 148, p. 257-274.

Schneiderhan, E. A., Gutzmer, J., Strauss, H., Mezger, K. and Beukes, N. J., 2006, The chemostratigraphy of a Paleoproterozoic MnF-BIF succession - the Voelwater Subgroup of the Transvaal Supergroup in Griqualand West, South Africa: South African Journal of Geology, v. 109, p. 63-80.

Schreiber, U. M. and Eriksson, P. G., 1992, The sedimentology of the post-Magaliesberg formations of the Pretoria Group, Transvaal Sequence, in the eastern Transvaal: South African Journal of Geology, v. 95, p.1-16.

Schröder, S., Bekker, A., Beukes, N. J., Strauss, H. and van Niekerk, H. S., 2008, Sulfate evaporites in the ~2.2–2.1 Gyr shallow-marine Lucknow Formation, South Africa: evidence for the rise in seawater sulfate concentration in association with the Paleoproterozoic positive carbon isotope excursion. Terra Nova, v. 20, (2), p. 108-117.

Sumner, D.Y., 2002, Neoarchean carbonates: Clues to early life and early ocean chemistry. Excursion Guide: 16th International Sedimentological Conference, International Association of Sedimentologists, Johannesburg, 24 p.

Sumner, D. Y. and Beukes, N. J., 2006, Sequence stratigraphic development of the

Neoarchean Transvaal carbonate platform, Kaapvaal Craton, South Africa: South African Journal of Geology, v. 109, p.11-22.

Sumner, D.Y. and Bowring, S. A., 1996, U-Pb geochronologic constraints on deposition of the Campbellrand Subgroup, Transvaal Supergroup, South Africa: Precambrian Research, v. 79, p. 25-35.

Sumner, D. Y. and Grotzinger, J. P., 2004, Implications for Neoarchaean ocean chemistry from primary carbonate mineralogy of the Campbellrand-Malmani Platform, South Africa: Sedimentology, v. 51, p. 1273-1299.

Swart, Q. D., 1999, Carbonate rocks of the Paleoproterozoic Pretoria and Postmasburg Groups, Transvaal Supergroup. MSc Thesis, Rand Afrikaans University, Johannesburg, 126 p.

Thode, H.G., Monster, J., and Dunford, H.B., 1961, Sulphur isotope geochemistry: Geochimica et Cosmochimica Acta, v. 25, p. 159–174, doi: 10.1016/0016-7037(61)90074-6.

Van Niekerk, H. S., 2006, The origin of the Kheis terrane and its relationship with the Archean Kaapvaal Craton and the Grenvillian Namaqua Province in southern Africa. PhD Thesis, University of Johannesburg, Johannesburg, 403 p.

Walraven, F., 1997, Geochronology of the Rooiberg Group, Transvaal Supergroup, South Africa. Economic Geology Research Unit Information Circular, University of the Witwatersrand, Johannesburg, 21 p.

Walraven, F. and Martini, J., 1995, Zircon Pb-evaporation age determinations of the Oak Tree Formation, Chuniesport Group, Transvaal Sequence: Implications for Transvaal-Griqualnd West basin correlations: South African Journal of Geology, v. 98, p. 58-67.

Table DR1: Results of elemental and isotopic analyses of samples from the Transvaal Supergroup, South Africa

Sample	lithology	Unit name	Age	$\delta^{33}S_{CAS}$	$\delta^{34}S_{CAS}$	$\delta^{36}S_{CAS}$	$\Delta^{33}S_{CAS}$	$\Delta^{36}S_{CAS}$	$\delta^{33}S_{CRS}$	$\delta^{34}S_{CRS}$	$\delta^{36}S_{CRS}$	$\Delta^{33}S_{CRS}$	$\Delta^{36}S_{CRS}$	$\delta^{13}C_{CARB}$	$\delta^{18}O_{CARB}$
			(Ma)	(‰, VCDT)										(‰, VPDB)	
Rie1-1	Stromatolitic imestone, contact metamorphism	Houtenbek Fm.	2100						3.400	6.572	12.56	0.021	0.04	-1.6	-18.1
Ven 6	Micritic dolomite	Lucknow Fm.	2161	7.134	13.897	26.26	0.001	-0.31						8.8	-9.3
Ven 5	Micritic dolomite	Lucknow Fm.	2162	6.706	13.084	24.73	-0.012	-0.27						9.1	-9.1
Ven 7	Micritic dolomite	Lucknow Fm.	2166	6.649	12.978	24.59	-0.014	-0.21						10	-8.6
Mog1	recrystallized dolomite, laminated	Silverton Fm.	2170	8.370	16.622	31.80	-0.156	-0.01	4.340	8.480	16.10	-0.018	-0.08	9.8	-12.9
Mog2	recrystallized dolomite, laminated	Silverton Fm.	2171	8.448	16.784	32.02	-0.161	-0.11	5.430	10.579	19.96	-0.005	-0.24	10	-13.4
Mog3	recrystallized dolomite, laminated	Silverton Fm.	2172	8.562	17.002	32.44	-0.158	-0.11	2.522	4.903	9.15	0.000	-0.24	9.6	-13.4

Mog4	recrystallized dolomite, laminated	Silverton Fm.	2173	7.918	15.575	29.42	-0.072	-0.38	3.577	6.970	13.10	-0.007	-0.18	9.7	-10.9
Mog5	recrystallized dolomite, laminated	Silverton Fm.	2174	6.015	11.822	22.40	-0.056	-0.18	-4.630	-9.057	-16.71	0.045	0.43	8.9	-12.3
M10-1	ferruginous dolomite, laminated	Mooidraai Fm.	2202						2.772	5.423	11.03	-0.017	0.7	-1.4	-9
M10-2	massive dolomite	Mooidraai Fm.	2201						-2.399	-4.570	-7.91	-0.043	0.76	-1.1	-6.4
M10-3	massive dolomite	Mooidraai Fm.	2200	10.096	19.694	37.91	0.002	0.16	7.980	15.578	29.99	-0.013	0.19	0.2	-3.1
M10-4	massive dolomite	Mooidraai Fm.	2200						-0.992	-1.942	-3.61	0.009	0.07	0.5	-2.1
M10-5	massive dolomite	Mooidraai Fm.	2200	15.403	30.220	58.28	-0.048	0.08	3.808	7.389	14.31	0.009	0.22	-0.1	-2.1
DF 21	massive dolomite	Duitschland Fm.	2321	12.850	25.042	48.5	0.031	0.4						6.5	-19.6
DF 22	fine-grained dolomite	Duitschland Fm.	2322	8.464	16.439	31.5	0.031	0.0						6.1	-16
DF 15	limestone with discontinuous	Duitschland Fm.	2323	10.513	20.435	39.3	0.041	0.1						7.8	-13.4

	slilceous layers															
DF 16	massive dolomite	Duitschland Fm.	2325	8.307	16.141	30.9	0.027	0.0						6.5	-13.4
DF 14	limestone with cm-sized cherty concretions	Duitschland Fm.	2330	11.955	23.285	44.9	0.030	0.2						1.6	-14
Dui13*	limestone/dolomite, laminated, serpentinized	Duitschland Fm.	2330	12.621	24.658	47.63	-0.003	0.26	8.780	17.099	32.76	0.010	0.02	6.8	-19.5
Dui12*	limestone/dolomite, laminated, serpentinized	Duitschland Fm.	2330	11.358	22.159	42.63	0.007	0.11						5.7	-19.5
Dui11*	limestone/dolomite, laminated, serpentinized	Duitschland Fm.	2330	9.504	18.494	35.48	0.022	0.05						6.7	-18.5
DF 13	limestone/dolomite, cm-scale cherty laminations, minor	Duitschland Fm.	2331	12.422	24.105	46.4	0.080	0.1						2.5	-10.4

DF 10	mineralized fractures laminated limestone, discontinuous cherty horizons	Duitschland Fm.	2338	14.210	27.704	53.6	0.037	0.3							3.8	-18.4
DF 20	massive dolomite	Duitschland Fm.	2342	21.682	42.302	82.5	0.115	0.6								
DF 19	stromatiolitic limestone	Duitschland Fm.	2344	14.549	28.271	54.7	0.088	0.3							6	-16.2
Dui5	stromatolitic limestone, locally cherty and cuprous	Duitschland Fm.	2349	12.687	24.655	47.51	0.064	0.15								
DF 8	nstromatolitic limestone, locally cherty and cuprous	Duitschland Fm.	2349	14.246	27.576	53.3	0.138	0.3							6.14	-16.67
Dui4	stromatolitic limestone, locally cherty and cuprous	Duitschland Fm.	2349						-0.087	-0.408	-1.18	0.123	-0.4		2.4	-10.9
DF 9	stromatolitic	Duitschland Fm.	2350	14.097	27.197	52.6	0.182	0.3							5.31	-17

Dui2	limestone stromatolitic limestone, locally cherty and cuprous	Duitschland Fm.	2350						-0.519	-1.476	-3.33	0.242	-0.53	2.6	-11.3
DF 5	siltstone with disseminated pyrite	Duitschland Fm.	2378						1.745	2.349	4.0	0.537	-0.4		
Dui14	sucrosic dolomite, massive	Duitschland Fm.	2381						5.512	9.389	16.68	0.688	-1.23	-1.7	-12.3
Dui15	stromatolitic dolomite	Duitschland Fm.	2382						-2.364	-6.154	-12.17	0.810	-0.51	1.9	-13.2
DF 18	massive dolomite	Duitschland Fm.	2382	3.373	6.166	11.8	0.203	0.0						0.01	-10.03
Dui16	sucrosic dolomite, massive	Duitschland Fm.	2383						5.107	8.718	15.72	0.627	-0.91	-1.4	-11.8
DF 4	cherty pelite with concentrations of pyrite	Duitschland Fm.	2385						3.232	3.984	6.2	1.183	-1.4		
Dui17	sucrosic	Duitschland Fm.	2385						2.363	3.069	4.80	0.784	-1.04	-1.4	-12.3

DF 2	dolomite, stromatolitic calcareous mudstone with concentrations of pyrite	Duitschland Fm.	2387						0.656	-1.457		1.407			
DF 3	calcareous mudstone with concentrations of pyrite	Duitschland Fm.	2387						3.583	4.462	7.0	1.288	-1.5		
Dui18	Calcareous mudstone	Duitschland Fm.	2388	4.963	8.072	14.47	0.814	-0.92	3.993	5.509	9.28	1.159	-1.21		
DF 17	massive limestone with minor chert layers	Duitschland Fm.	2388	5.518	9.287	17.0	0.746	-0.7						-1.71	-11.02
DF 1	calcareous mudstone with concentrations of pyrite	Duitschland Fm.	2390						3.343	5.359		0.586			
DF 28	laminated mudstone	Duitschland Fm.	2390						2.968	5.411	10.0	0.185	-0.3		
Koe 4*	ferruginous	Koegas Fm.	2415	2.858	4.683	8.28	0.449	-0.64	1.943	0.741	-0.54	1.562	-1.95	-10.8	-18.6

Koe 2*	cherty sucrosic dolomite, strong recrystallization ferruginous cherty sucrosic dolomite, strong recrystallization	Koegas Fm.	2420						1.809	3.379	6.53	0.070	0.09	-9	-17
San 2*	ferruginous limestone, sparitic, stromatolitic	Koegas Fm.	2430											-5.6	-13.6
Ton7	stromatolitic dolomite	Tongwane Fm.	2435						10.705	20.668	39.88	0.114	0.25	-0.8	-11.9
Ton2*	ferruginous dolomite, recrystallized	Tongwane Fm.	2437						-1.365	-1.960	-3.68	-0.355	0.04		
TR01-C	massive dolomite overlying chert breccia	Tongwane Fm.	2439	9.658	18.584	36.0	0.130	0.4							
Gla 21	Ferruginous	Gamohaan Fm.	2505						7.598	4.896	4.25	5.080	-5.08	-0.3	-8.1

DF23-C	limestone, recrystallized, laminated massive dolomite	Malmani Subgroup	2525	6.412	10.453		1.042								
DF27-C	massive dolomite with minor chert layers	Malmani Subgroup	2550	9.057	14.427	26.4	1.653	-1.2							
DF26-C	laminated dolomite interbedded with chert	Malmani Subgroup	2560	8.445	10.914	18.8	2.839	-2.0							
Nau 6	Ferruginous dolomite, stromatolitic	Nauga Fm.	2570						8.979	3.274	-0.36	7.295	-6.59		
Bav4	stromatolitic limestone	Reivilo Fm.	2580						15.325	11.199	11.89	9.573	-9.49	-0.5	-10.4
Mon 6	Cross bedded limestone	Monteville Fm.	2600						9.706	14.800	25.56	2.111	-2.75	-0.5	-9.8
Boo 1	Oolitic dolomite	Boomplaas Fm.	2615						2.467	1.013	0.60	1.945	-1.33	0.3	-11.3

*sample visibly altered